Science of the Total Environment 996 (2025) 180122

Contents lists available at ScienceDirect

Science of the Total Environment

journal homepage: www.elsevier.com/locate/scitotenv

Empirical approaches to estimate rainfall erosivity from coarse temporal resolution precipitation data in the Mediterranean region

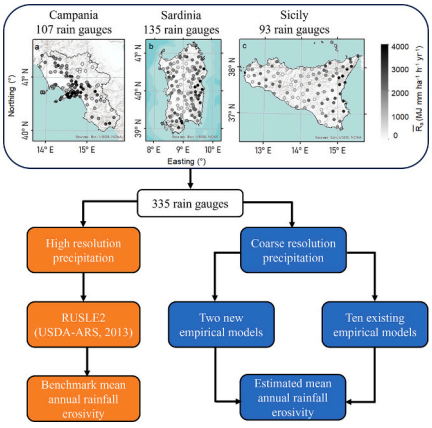
Surafel M. Woldegebrael [a], Nunzio Romano [a], Dario Pumo [b], Roberto Deidda [c], Matteo Ippolito [b], Marcella Cannarozzo [b], Andreas Langousis [d], Athanasios V. Serafeim [c,e], Salvatore Manfreda [f], Paolo Nasta [a,*]

[a] Department of Agricultural Sciences, University of Naples Federico II, Portici, Napoli, Italy
[b] Department of Engineering, University of Palermo, Palermo, Italy
[c] Department of Civil and Environmental Engineering and Architecture, University of Cagliari, Cagliari, Italy
[d] Department of Civil Engineering, University of Patras, Greece
[e] Department of Civil Engineering, University of Peloponnese, Patras, Greece
[f] Department of Civil, Architectural and Environmental Engineering, University of Naples Federico II, Napoli, Italy

HIGHLIGHTS

- Two empirical models were developed in southern Italy to estimate erosivity.
- The first equation uses the rainfall episodicity and intensity indices.
- A refined variant also considers geographic and terrain covariates.
- The proposed models outperformed ten existing simplified models locally recalibrated.

GRAPHICAL ABSTRACT



ARTICLE INFO

Keywords:
Soil erosion
RUSLE
R factor
Daily rainfall erosivity models
Gini's coefficient

ABSTRACT

The assessment of rainfall erosivity is often hindered by the limited availability of high-resolution rainfall data. A large dataset, comprising 10-minute rainfall data collected over the last two decades from 335 rain gauges across three regions of southern Italy, was utilized in this study to estimate benchmark values of mean annual rainfall erosivity according to the Revised Universal Soil Loss Equation. A set of ten existing simplified models based on coarser resolution rainfall data (from daily to annual) were compared to two newly developed empirical models based on daily-resolution data. The first proposed model uses two compound meteorological predictors, namely the rainfall episodicity and intensity indices, derived from the mean annual rainfall, the Gini's coefficient, and the mean annual number of rainy days. The second model integrates the previous one with geographic and

* Corresponding author.
E-mail address: paolo.nasta@unina.it (P. Nasta).

https://doi.org/10.1016/j.scitotenv.2025.180122
Received 28 January 2025; Received in revised form 8 July 2025; Accepted 19 July 2025
Available online 28 July 2025
0048-9697/© 2025 The Authors. Published by Elsevier B.V. This is an open access article under the CC BY license (http://creativecommons.org/licenses/by/4.0/).

topographic covariates, including latitude, elevation, and minimum distance to the coastline. We evaluated and compared the performances of all models using various metrics, including the Root Mean Square Error (RMSE), the mean error, the adjusted coefficient of determination, the Kling-Gupta efficiency, and the Akaike information criterion. All the performance indices showed how the newly developed models outperformed the ten existing recalibrated equations, obtaining a reduction in absolute percentage error from 27 to 18 %. Our extensive dataset enabled robust calibration and validation of existing and new simplified models, paving the way for an ensemble modeling approach that enhances model transferability in data-scarce environments under similar precipitation regimes.

1. Introduction

Land degradation is a major environmental threat that undermines the provision of essential ecosystem services throughout Europe (Prăvălie et al., 2024). An ambitious plan to tackle environmentally harmful soil degradation processes, especially in southern Europe, has been laid out in the newly announced European Green Deal (Panagos et al., 2015a; Montanarella and Panagos, 2021; Panagos et al., 2024). Water-induced soil erosion is regarded as a principal indicator for the implementation of the Common Agricultural Policy and the Farm to Fork strategy within the European Union (Montanarella and Panagos, 2021). Understanding the reliability of models in estimating soil erosion processes is essential for the implementation of sustainable land management and conservation efforts. This is especially important in light of global change, specifically the seasonality of rainfall and the rapid changes in land use, both of which are already having a noticeable impact in many parts of the world, like the Mediterranean region (Noto et al., 2023a,b; Avino et al., 2024).

The Revised Universal Soil Loss Equation (RUSLE) is an empirical model that estimates the mean annual soil loss from raindrop splash and runoff from hillslopes at large spatial scales (Nearing et al., 2017; Benavidez et al., 2018). In RUSLE, soil loss due to rill and interrill erosion is estimated from the product of the rainfall erosivity factor (R), the soil erodibility factor (K), the slope length and steepness factor (LS), the crop type and management factor (C), and the supporting conservation practices factor (P). Rainfall erosivity plays a crucial role in both the Revised Universal Soil Loss Equation (RUSLE) and its predecessor, the Universal Soil Loss Equation (USLE; Wischmeier and Smith, 1978), because precipitation initiates soil erosion and directly affects the detachment and movement of soil particles by runoff.

The R-factor is a multi-annual average index that accounts for the effects of kinetic energy and intensity of precipitation on soil erosion. The conventional method for calculating rainfall erosivity is based on the original protocol proposed by Wischmeier and Smith (1978), which requires high-resolution rainfall data which are crucial particularly in the Mediterranean region where erosivity is dominated by short, intense convective rainfall (Piccarreta et al., 2024). Accurate mapping of the R-factor represents the final product for effective soil conservation and land management (Panagos et al., 2015b). However, simplified empirical equations based on more readily available coarser resolution rainfall datasets (e.g., daily, monthly, or annual) retrieved from high-density rain gauge networks (Bonilla and Vidal, 2011; Padulano et al., 2021) are often used in regions with limited (or null) availability of high-resolution rainfall data. Yin et al. (2017) highlight how scarcity of high-resolution data compromises the accurate mapping of the R-factor over large territories and hinders the analysis of temporal patterns. Unfortunately, empirical equations suffer from significant limitations. First, empirical equations are formulated by analyzing the relationship between rainfall and erosivity within a specific geographic area and time frame. Consequently, the coefficients and parameters derived from this analysis are specifically tailored to the local rainfall regime and the period considered, making them non-transferable to significantly different geographic locations or temporal contexts. Second, a significant limitation arises from the inherent information loss associated with the use of aggregated rainfall data. Rainfall erosivity is highly dependent on the kinetic energy of raindrops, which is directly influenced by rainfall intensity and duration. The use of monthly or annual rainfall data may obscure critical details of individual rainfall events. For instance, a high annual rainfall total may result from either numerous low-intensity events or a few very intense storms concentrated in a short period of the year. The latter scenario would exhibit significantly greater erosive potential; however, methodologies based solely on monthly or annual rainfall data would fail to capture these critical differences in rainfall erosivity. Although daily-resolution data offer an improvement over monthly or annual data, they remain insufficient for fully capturing the complexity of erosive events. The performance of empirical equations based on daily rainfall has been enhanced through the development of more sophisticated models, incorporating month-to-month calibration (Angulo-Martínez and Beguería, 2009). However, there is still room to incorporate key information on daily rainfall distribution by striking the balance between model complexity and the level of detail available at daily resolution.

The primary aim of this study is to assess the generalizability of existing and new empirical relationships for estimating the mean annual R-factor based on rainfall data with coarse temporal resolution in the Mediterranean region.

The present study focuses on an area of 63,600 km^2 encompassing the southern Italian regions of Campania, Sicily, and Sardinia. The analysis is based on 10-minute rainfall data collected between 2004 and 2023 from a dense network of 335 rain gauges, with an average of one station per 190 km^2. Rainfall erosivity was estimated using the methodology originally developed by Wischmeier and Smith (1978) and later revised by USDA–ARS (2013). The availability of high-resolution rainfall data with significant temporal and spatial coverage across the study area, served as an invaluable resource for this study. To achieve the primary aim, the study set the following objectives:

- Derive and analyze an extensive dataset of benchmark mean annual rainfall erosivity values, obtained from 10-min resolution data across the study area.
- Calibrate and validate ten existing empirical equations for estimating mean annual rainfall erosivity using coarse resolution rainfall data (daily, monthly and annual sums).
- Develop, calibrate and validate a new parsimonious equation based on daily rainfall data, incorporating two rainfall-related indices that effectively represent the influence of rainfall intensity and its distribution throughout the year on mean annual rainfall erosivity.
- Further refine this new equation by integrating easily retrievable terrain and geographic features, including elevation, latitude, minimum distance to coastline, slope, and aspect.
- Evaluate and compare the performance of the existing simplified equations (both in their original form and after local recalibration) with the newly developed equations, assessing their strengths and limitations based on their complexity and accuracy relative to the benchmark erosivity values.

2. Materials and methods

2.1. Rain gauge networks in the pilot regions

This research is part of the Project ASAP (*Assessing and Mapping Novel Agroecosystem Vulnerability and Resilience Indicators in Southern Italy*) financed by European Union —NextGenerationEU, which identified three Italian regions particularly vulnerable to water-related natural hazards as pilot study areas. By selecting three distinct regions to represent the diverse climatic and geographical conditions of the southern Mediterranean, we aimed to gain a nuanced understanding of how different rainfall regimes and terrain characteristics impact erosivity and the performance of estimation equations. Analyzing the specific characteristics of each region, such as rainfall patterns, topography, and proximity to the sea, offers deeper insights into the factors governing the accuracy and applicability of the tested empirical equations. The three pilot regions under consideration, located in southern Italy, are Campania, Sardinia, and Sicily, with surface areas of 13,668 km^2, 24,106 km^2, and 25,824 km^2, respectively. The Köppen-Geiger classification designates the climate of these regions as Csa (*Warm temperate climate with hot dry summer*) (Kottek et al., 2006). Snowfall is rare in the coastal zones of these three regions, with seasonal occurrence at high inland elevations. The precipitation regime is marked by a pronounced seasonality, with predominantly frontal rainfall in winter and convective rainfall in summer. The variability of precipitation characteristics across each region is strongly influenced by orographic effects and the proximity to the Mediterranean Sea.

A total of 107, 135, and 93 automated rain gauges in Campania, Sardinia, and Sicily, respectively, were used to track rainfall data at a 10-minute resolution. Data from Campania were obtained from the *Centro Funzionale per la Previsione Meteorologica e il Monitoraggio Meteo-Idro-Pluviometrico e delle Frane della Regione Campania* website (https://centrofunzionale.regione.campania.it/#/pages/dashboard). The dataset for Sicily was retrieved from the SIAS (*Servizio Informativo Agrometeorologico Siciliano*) regional agency, whereas that for Sardinia from the *Agenzia Regionale per la Protezione dell'Ambiente della Sardegna* (https://arpas.maps.arcgis.com/home/index.html). The average density of rain gauges is one station per 128 km^2, 192 km^2, and 256 km^2 in Campania, Sardinia, and Sicily, respectively, denoting appreciable and homogeneous spatial coverage in all three regions. The three regional datasets used in the analysis encompass the same timeframe, extending from 2004 to 2023. The data from all the 335 rain gauges were split into two subsets: a calibration set, which includes data from 251 rain gauges, and a validation set, which consists of the remaining 84 rain gauges. The process of data splitting was carried out by ensuring equal representation of the three regions in the validation set, which is formed by data from 28 rain gauges per region. Fig. 1 illustrates the locations of the rain gauges within both datasets. The figure indicates that the rain gauges in both subsets are evenly distributed over the three regions. A 30-m resolution Digital Elevation Model (DEM) was downloaded from the publicly available U.S. Geological Survey's (USGS) EarthExplorer platform (Shuttle Radar Topography Mission 1 Arc-Second Global dataset, https://earthexplorer.usgs.gov/). The following terrain and geographic features, useful for the conducted analyses, were retrieved for each rain gauge: elevation (*Z*); minimum distance from the sea (*DS*); slope (*SL*); aspect (*AS*); and latitude (*Lat*).

2.2. Definition of benchmark rainfall erosivity based on high-resolution rainfall data

Rainfall erosivity, also known as the R-factor, is an indicator that quantifies the erosive potential of raindrops, dependent on the duration, magnitude, and intensity of erosive storms (Wischmeier and Smith, 1978; Panagos et al., 2015a). The calculation of this factor requires the preliminary identification of erosive rainfall events (Renard et al., 1997). Wischmeier and Smith (1978) developed a method for

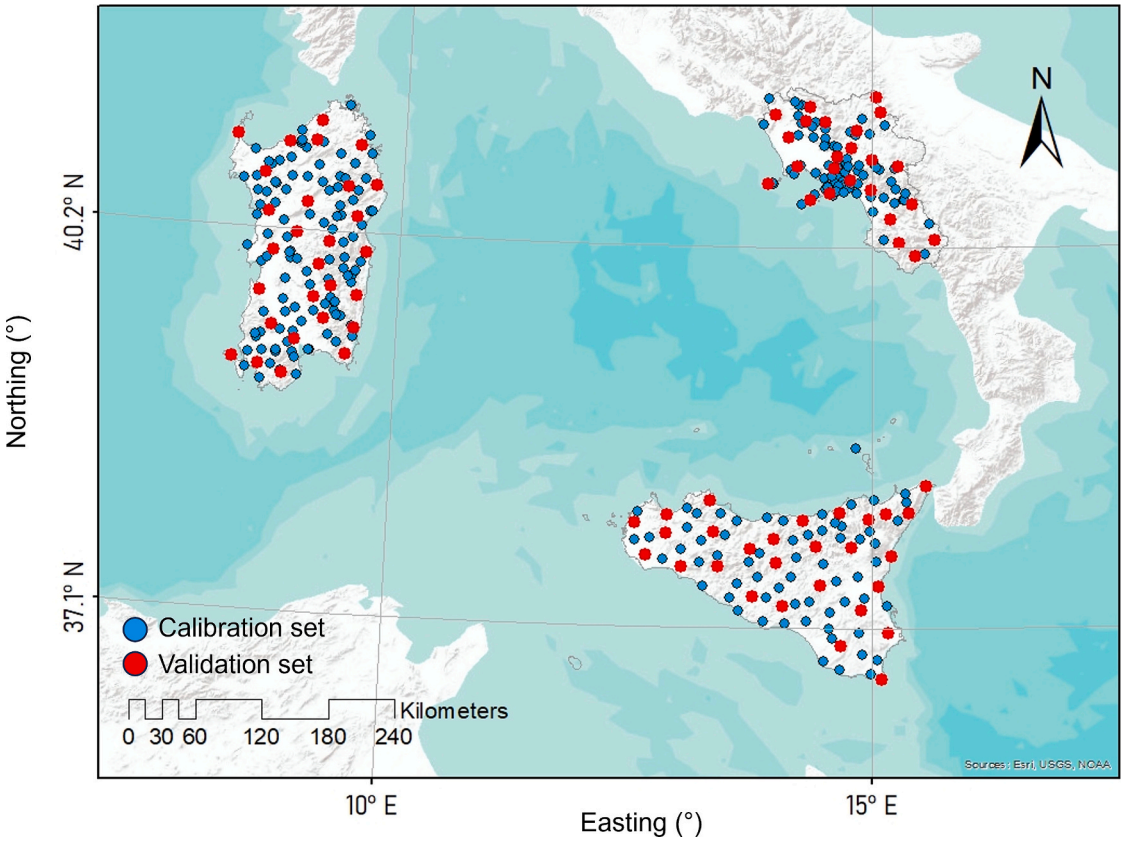


Fig. 1. Rain gauge locations in Campania, Sardinia, and Sicily. The 30-m resolution Digital Elevation Model (DEM) is shown as a hillshade map.

identifying an erosive storm event based on the following criteria: *i*) a storm is classified as erosive if its cumulative rainfall is greater than 12.7 mm (i.e., 0.5 in.), or if it exhibits a rainfall intensity peak exceeding 6.35 mm (i.e., 0.25 in.) in 15 min; and *ii*) individual storms are defined considering a minimum inter-event time of 6 h with cumulative rainfall lower than 1.27 mm (i.e., 0.05 in.).

For each erosive storm that meets the criteria outlined by Wischmeier and Smith (1978), the R-factor of single events, R_s (MJ mm ha^{-1} h^{-1}), is calculated as the product of the storm kinetic energy, E (MJ ha^{-1}), and the storm maximum 30-min intensity during the event, I_{30} (mm h^{-1}):

$$R_s = (E{\cdot}\mathrm{I}_{30})_s = \left[\left(\sum_{r=1}^{n} e_r v_r\right){\cdot}I_{30}\right]_s \quad (1)$$

where the storm kinetic energy E is computed by first dividing the storm into n time intervals (in this study we used a regular 10-min time step), and then summing the products of the rainfall energy per unit rainfall e_r (MJ ha^{-1} mm^{-1}) by the rainfall depth v_r (mm) in each interval (where $r = 1, \ldots, n$ is the generic interval throughout the storm event). The term e_r in each time interval is computed as a function of the rainfall intensity, i_r (mm h^{-1}) for the same interval, as proposed by USDA–ARS (2013) in the RUSLE2 which represents an updated version of the RUSLE originally presented by Renard et al. (1997):

$$e_r = 0.29{\cdot}[1 - 0.72{\cdot}exp(-0.082{\cdot}i_r)] \quad (2)$$

The rainfall erosivity at a certain location is typically expressed as monthly rate by *i*) first summing all single-storm rainfall erosivity events (R_s), computed at storm event scale by Eq. (1), in each month, and then *ii*) averaging the results over all months in the record. The resulting mean monthly rainfall erosivity, $\overline{R}_m$, is thus expressed as MJ mm ha^{-1} h^{-1} month^{-1}. The same approach is used to obtain the mean annual rainfall erosivity ($\overline{R}_a$ in MJ mm ha^{-1} h^{-1} yr^{-1}) assumed as benchmark R-factor value in this study.

2.3. Empirical equations to estimate the R-factor based on coarse rainfall data

This study explores the use of ten empirical equations for estimating the mean annual rainfall erosivity ($\overline{R}_a$) using predictors derived from rainfall data with daily or coarser time resolution (Table 1). The equations FER2003, NAK2014, PAD2021, Y&R1996 in Table 1 are based on the mean annual precipitation (*MAP*). PAD2021 exploits also elevation (Z in m a.s.l.) and latitude (*Lat* in °N referring to the WGS84 UTM coordinate system) as terrain and geographical covariates. Y&R1996 was calibrated in Australia (Yu and Rosewell, 1996a) and China (Zhu and Yu, 2015) and resorts to the analytical equation originally proposed by Renard and Freimund (1994) in continental USA.

The equations R&F1994, ZHO1995, OZS2012, FER1999 in Table 1 use mean monthly rainfall data (MMP_m), either directly, as in ZHO1995, or indirectly, as in R&F1994 and OZS2012, which rely on the Modified Fournier Index (*MFI*), calculated based on MMP_m. FER1999 adopts a variant of the Modified Fournier Index (F_F) which quantifies the impact of monthly rainfall variability on the R-factor through the coefficient of variation (CV) of monthly precipitation (*MP*).

The equations F&P2014 and P&M2004 in Table 1 were applied in Mediterranean climate regions (Portugal and Slovenia) and rely on daily rainfall data to compute the mean monthly rainfall erosivity values ($\overline{R}_m$), and, then, the $\overline{R}_a$ by summing $\overline{R}_m$ over all months of the year. F&P2014 adopts the analytical form originally proposed by Goovaerts (1999), which was also used in Loureiro and Coutinho (2001) in the Algarve region (Portugal). The F&P2014 model employs two predictors, namely MMP_{10} and $\overline{d}_{10,m}$, which are retrieved from the analysis of daily rainfall data in rainy erosive days with daily rainfall above 10 mm. MMP_{10} and $\overline{d}_{10,m}$ denote the mean monthly rainfall and the mean number of rainy erosive days in month m, respectively. P&M2004 adopts an exponential analytical form, originally proposed by Richardson et al. (1983), based on two empirical parameters (a and b), even if, for the sake of simplicity, the exponent b is often directly assumed to be equal to 2, resulting in a mono-parametric model. As for the previous model, also P&M2004 is based on the analysis of daily rainfall in rainy erosive days with rainfall

Table 1
List of the ten empirical equations selected to estimate the mean annual rainfall erosivity, $\overline{R}_a$ (MJ mm ha^{-1} h^{-1} yr^{-1}), with original references, assigned acronyms, description of predictors, and indication of the location where they were calibrated. $\overline{R}_m$ (MJ mm ha^{-1} h^{-1} month^{-1}) is the mean monthly erosivity. AP_y, *MAP* and MMP_m indicate the annual precipitation at year y, the mean annual precipitation and the mean monthly precipitation at month m, respectively. Y refers to the total number of years of records. $CV^2(MP)_y$ is square of the coefficient of variation of monthly rainfall at the generic year y. Z the elevation (m a.s.l.), and *Lat* the latitude (°N referring to the WGS84 UTM coordinate system). *MFI* is the Modified Fournier Index (mm), while F_F is its modified version in Ferro et al. (1999). Rainy erosive days are defined as days with rainfall exceeding 10 mm. $P_{10,k}$ indicates daily rainfall at the k-th rainy erosive day, and D_m is the total number of rainy erosive days in month m. MMP_{10} and $\overline{d}_{10,m}$ are the mean monthly rainfall and the mean number of rainy erosive days in month m, respectively. The parameters of all models are indicated by a, b, c, and d.

Acronym	Reference	Equation	Predictors	Original location
FER2003	Fernandez et al. (2003)	$\overline{R}_a = a + b{\cdot}MAP$	*MAP*	USA
NAK2014	Nakil (2014), as cited in Nakil and Khire (2016)	$\overline{R}_a = a{\cdot}e^{b{\cdot}MAP}$	*MAP*	India
PAD2021	Padulano et al. (2021)	$\overline{R}_a = \frac{MAP^a}{b + Z^c{\cdot}Lat^d}$	*MAP, Z, Lat*	Italy
Y&R1996	Yu and Rosewell (1996b)	$\overline{R}_a = a{\cdot}MAP^b$	*MAP*	USA
R&F1994	Renard and Freimund (1994)	$\overline{R}_a = a + b{\cdot}MFI + c{\cdot}MFI^2$ $MFI = \sum_{m=1}^{12}\frac{MMP_m^2}{MAP}$	*MAP, MMP*$_m$	USA
ZHO1995	Zhou et al. (1995)	$\overline{R}_a = \sum_{m=1}^{12}(a + b{\cdot}MMP_m)$	MMP_m	China
OZS2012	Ozsoy et al. (2012)	$\overline{R}_a = a{\cdot}MFI^b$ $MFI = \sum_{m=1}^{12}\frac{MMP_m^2}{MAP}$	*MAP, MMP*$_m$	Turkey
FER1999	Ferro et al. (1999)	$\overline{R}_a = a{\cdot}F_F^b$ $F_F = \frac{1}{Y}\sum_{y=1}^{Y}\frac{AP_y}{12}\left[1 + CV^2(MP)_y\right]$	AP_y, $CV^2(MP)_y$	Italy
F&P2014	Ferreira and Panagopoulos (2014)	$\overline{R}_m = a{\cdot}MMP_{10} + b{\cdot}\overline{d}_{10,m}$	MMP_{10}, $\overline{d}_{10,m}$	Portugal
P&M2004	Petkovšek and Mikoš (2004)	$\overline{R}_m = a\frac{1}{D_m}\sum_{k=1}^{D_m}P_{10,k}^2$	$P_{10,k}$	Slovenia

exceeding 10 mm.

The ten existing empirical equations in Table 1 were tested with their original parameterization and also considering a local recalibration on the study area (see Section 2.5) to ensure a fair comparison between the existing and the new models proposed in this study.

2.4. Other predictors for estimating the mean annual rainfall erosivity

Two rainfall-based compound predictors were derived from the analysis of daily rainfall data exceeding 10 mm ($P_{10,k}$), which were considered as rainy erosive days, in accordance with the methodologies used in the F&P2014 and P&M2004 equations. Specifically, these predictors were based on: *i*) the mean annual rainfall computed over rainy erosive days, MAP_{10}, *ii*) the mean annual number of rainy erosive days $\overline{d}_{10,a}$, and, *iii*) the mean annual Gini's coefficient (G) computed for erosive days (Gini, 1914).

Gini's coefficient (G) is a statistical metric used to quantify inequality within a statistical distribution and ranges from 0 to 1, with 0 representing perfect equality (i.e., an equi-distribution along a 1:1 line on the Lorentz curve, with rainy erosive days equally contributing to the total rainfall) and 1 representing extreme inequality (i.e., maximum concentration, with the total annual rainfall occurring in a single rainy day), respectively. The calculation of G can be performed according to the following steps (Nasta et al., 2018): 1) ranking the rainy erosive days in ascending order of daily rainfall ($P_{10,k}$); 2) deriving the relative frequency distribution by using a plotting position, i.e., $p_i = i/N$ for the i-th ranked rainy erosive day, where N is the total number of rainy erosive days; 3) computing q_i, i.e. the proportion of cumulative rainfall at the i-th ranked rainy erosive day over the total rainfall, given by $q_i = \sum_{k=1}^{i} P_{10,k} / \sum_{k=1}^{N} P_{10,k}$. The Gini's coefficient is then defined as follows (Deltas, 2003):

$$G = \frac{\sum_{i=1}^{N-1}(p_i - q_i)}{\sum_{i=1}^{N-1} p_i} \tag{3}$$

The two new compound predictors investigated for the development of new empirical equations are defined as:

1) Rainfall Episodicity Index: REI = $MAP_{10} \cdot G$;
2) Rainfall Intensity Index: RII = $MAP_{10} / \overline{d}_{10,a}$.

Gini's coefficient contributes to the assessment of the mean annual R-factor by weighing the MAP_{10} values in the REI. In other words, high REI values are obtained with few episodic rainfall events throughout the year (i.e., for G close to 1), while low REI values are derived from frequent rainfall events throughout the year (i.e., for G close to 0). Likewise, a high RII means that the annual erosive rainfall values are concentrated within a few days making them more erosive than they would be if the RII was low. The main hypothesis is that high values of REI and/or RII are linked to high $\overline{R}_a$. The model calibration process is made easier by using REI and RII as measures for the distribution of rainfall-induced erosion events over the course of the year, eliminating the need for computation of mean monthly R-factors prior to obtaining mean annual R-factors, which are necessary for both models based on daily rainfall data, namely F&P2014 and P&M2004.

The observed variability of $\overline{R}_a$ across different sites within the same region could be also attributed to the influence of different terrain features on local rainfall patterns. Indeed, the Mediterranean region is characterized by mountainous landscapes, where orographic effects can strongly impact precipitation intensity, especially close to the coastal areas, where the sea could feed rainfall generation mechanisms. Moreover, aspect has potential influences on rainfall erosivity, since the south-facing slopes in the northern hemisphere receive more direct sunlight leading to warmer temperatures, which in turn increase evaporation rate, affecting atmospheric moisture content and potentially affecting storm patterns. Convective storms are characterized by rising warm air, often triggered by differences in temperature and moisture: vertical temperature and moisture profiles are strongly influenced by the elevation, aspect, slope, the location relative to the sea and mountains, and the latitude.

For this reason, we also tested possible improvements that can be achieved by including additional geographic and terrain features, i.e. the elevation (Z) and latitude (Lat) as in the PAD2021 model (see Table 1), as well as the minimum distance from the sea (DS), slope (SL), and aspect (AS).

2.5. Development of new empirical equations for the study area

A regression analysis was performed to evaluate the possible underlying relationship between the mean annual rainfall erosivity ($\overline{R}_a$) and the predictors discussed in the previous section. We considered benchmark $\overline{R}_a$ values, computed using 10-min resolution rainfall data according to the procedure in Section 2.2. Then, two families of regression equations were then developed based on the calibration dataset and evaluated over the validation dataset.

A family of regression models based on a parsimonious approach was first developed by using only the two proposed compound rainfall-based predictors (i.e., REI and RII). Linear and nonlinear regression models were tested by considering, both separately and in combined forms, REI and RII. The analytical forms of the multiple linear and nonlinear regression equations can be written generically as:

$$\overline{R}_a = \beta_1 + \beta_2 x_1 + \beta_3 x_2 \tag{4}$$

and

$$\overline{R}_a = \beta_1 x_1^{\beta_2} \cdot x_2^{\beta_3} \tag{5}$$

where x_p and β_p are the p-th predictors and parameters, respectively. Eq. (4) was also tested with null intercept (β_1=0). The trial-and-error method outlined below was used to choose the optimal formulation. We named the best model derived under the family of parsimonious approaches as ASAP1, based on the acronym of the project that funded this work.

Another family of regression models was subsequently developed, characterized by a more comprehensive approach that accounts for geographic and terrain features as additional predictors. This approach represents a refinement of ASAP1, and it was obtained by exploring all the possible combinations of five geographic and terrain features (i.e., Z, Lat, DS, AS, and SL), allowing also for their logarithmic transformations. A total of 242 different combinations were evaluated using multiple linear and nonlinear regression equations, employing the analytical forms in Eqs. (4) and (5). As with ASAP1, we identified ASAP2 as the best rainfall erosivity model derived under this second family of more complex approaches.

The parameters of all empirical models, including those in Table 1, were calibrated by solving a nonlinear least-squares data fitting algorithm (*lsqnonlin* function in Matlab). A bootstrap approach was used by randomly generating 1000 different calibration subsets. Each calibration subset was generated considering data from 195 rain gauges (65 per region) randomly selected from the 251 gauges forming the calibration dataset. Consequently, the optimization led to 1000 different optimal parameter sets for each model. The final parameter set of each model was determined by computing the ensemble mean of each parameter across all 1000 optimized sets. The performances of the models with the final parameter sets (and also with the original parameterization for the models in Table 1) were then assessed on the validation dataset ($n = 84$) based on a set of performance indicators, which are detailed in the following section.

Finally, in regression analysis, verifying some key assumptions is essential to ensure the reliability and validity of the resulting model.

These assumptions include the relationship type (linearity or log-log-linearity for the regression model in Eq. 5), homoscedasticity, normality of residuals, low multicollinearity and the absence of measurement errors in predictors. With this aim, the first and second assumptions were verified by analyzing residual plots, normality was tested using the Kolmogorov-Smirnov test (*kstest* function in MATLAB) at the 5 % significance level, while the assumption of low cross-correlation between predictors was tested using the Pearson correlation coefficient (r) and the Variance Inflation Factor ($VIF = 1 / 1 - R^2$), based on the knowledge of the coefficient of determination R^2.

2.6. Performance indicators

The performance of the various models tested in this study was evaluated through different indicators based on the comparison between $\overline{R}_a$ values simulated via simplified equations (Table 1 and newly proposed equations). The benchmark values were obtained considering 10-min rainfall data through the procedure described in Section 2.2.

The adopted performance indicators include the adjusted coefficient of determination (R^2_{adj}), the root mean square error (*RMSE*), the mean error (*ME*), the Kling-Gupta Efficiency (*KGE*), and the Akaike Information Criterion (*AIC*).

The adjusted coefficient of determination, R^2_{adj}, is defined as:

$$R^2_{adj} = 1 - \left(1 - R^2\right)\frac{n-1}{n-1-p} \tag{6}$$

where R^2 is the coefficient of determination defined as:

$$R^2 = 1 - \frac{\sum_j^n \left(O_j - E_j\right)^2}{\sum_j^n \left(O_j - \mu_O\right)^2} \tag{7}$$

The indicators *RMSE* and *ME* are defined as:

$$RMSE = \sqrt{\sum_j^n \frac{\left(E_j - O_j\right)^2}{n}} \tag{8}$$

$$ME = \sum_j^n \frac{\left(E_j - O_j\right)}{n} \tag{9}$$

The Kling-Gupta Efficiency, *KGE*, is given by:

$$KGE = 1 - \sqrt{(r-1)^2 + (\alpha - 1)^2 + (\beta - 1)^2}, \tag{10}$$

where r is the Pearson correlation coefficient, α is a bias term, and β denotes the variability of prediction errors. The terms r, α, and β are defined as:

$$r = \frac{cov(\mathrm{O}, \mathrm{E})}{\sigma_O^2 \sigma_E^2} \tag{11a}$$

$$\alpha = \frac{\mu_E}{\mu_O} \tag{11b}$$

$$\beta = \frac{\sigma_E}{\sigma_O} \tag{11c}$$

The Akaike Information Criterion (*AIC*) is calculated as follows:

$$AIC = n \times ln\left(\frac{SSE}{n}\right) + 2p \tag{12}$$

where SSE is the sum of squared errors, which is defined as:

$$SSE = \sum_j^n \left(E_j - O_j\right)^2. \tag{13}$$

In Eqs. (6)–(13), j refers to the specific rain gauge, n is the total number of rain gauges, O_j and E_j are the benchmark and simulated, respectively, values of the variable under analysis ($\overline{R}_a$) at the j-th station, μ_O and μ_E are their mean values across all stations, σ_O and σ_E are their standard deviations, and p is the number of parameters.

The term "perfect matching" is denoted by 1 for R^2_{adj} and zero for *RMSE* and *ME*. Negative or positive values of *ME* indicate under or overestimation, respectively. The *KGE* ranges from -∞ to 1, with 1 denoting optimal performance. The model with the smallest AIC value is considered to have the optimal fit.

3. Results

3.1. Analysis of rainfall erosivity from high-resolution rainfall

The annual rainfall values range from 655 to 1849 mm in Campania, from 306 to 1303 mm in Sardinia, and from 474 to 1370 mm in Sicily, with spatial-average values of 1181, 658, and 709 mm in Campania, Sardinia, and Sicily, respectively. The application of the RUSLE model to 10-minute precipitation data from 335 rain gauges resulted in the identification of 94,081 erosive events (49,441 in Campania, 23,788 in Sardinia, and 20,852 in Sicily).

Fig. 2 illustrates the spatial distribution of the benchmark $\overline{R}_a$ values in the three pilot regions; the resulting spatial averages of $\overline{R}_a$ were 3003, 1216 and 1801 MJ mm ha^{-1} h^{-1} yr^{-1} in Campania, Sardinia, and Sicily, respectively. The spatial variability across each region was quantified by using the coefficient of variation, which was 38.7 %, 48.4 %, and 46.8 % in Campania, Sardinia, and Sicily, respectively. It is worth noting that the spatial average $\overline{R}_a$ over all the 335 rain gauges in the three regions was 1949 MJ mm ha^{-1} h^{-1} yr^{-1} with CV of 59.5 %, indicating high variability of the $\overline{R}_a$ in the entire dataset.

The spatial patterns of $\overline{R}_a$ reflect those of the mean annual rainfall, although the R-factor is also dependent on precipitation's seasonal distribution (Fiener et al., 2013; Johannsen et al., 2022). In this regard, the spatial distribution of the monthly rainfall erosivity values ($\overline{R}_m$) is illustrated in Fig. 3 in the form of boxplots to help visualize the seasonal variability of the R-factor.

The characteristic seasonal precipitation pattern of Mediterranean coastal areas significantly influences the distribution of the monthly R-factor, R_m. The most critical months are September, October, and November, which mark the transition from late summer to fall. The highest R_m values were observed in November in both Campania and Sardinia, with mean values, $\overline{R}_m$ for Campania (i.e., 567 MJ mm ha^{-1} h^{-1} month^{-1}) about two times that in Sardinia (i.e., 243 MJ mm ha^{-1} h^{-1} month^{-1}). In Sicily, the highest $\overline{R}_m$ values were observed in October, with a mean value of 418 MJ mm ha^{-1} h^{-1} month^{-1}. However, a large variability of $\overline{R}_m$ values was observed in the period between September and November for all regions, indicating the occurrence of local events with R_m values exceeding 1000 MJ mm ha^{-1} h^{-1} month^{-1}.

A comparison of the monthly $\overline{R}_m$ in the three regions reveals that Campania exhibits significantly higher and more variable $\overline{R}_m$ values across stations compared to the other two regions for all months. Sardinia is typically characterized by aridity, even during the rainy season (Ballabio et al., 2017), and this was reflected in the low $\overline{R}_m$ values for the winter months compared to the other two regions.

In all regions, summer and fall storms are mainly characterized by high intensity and short duration, originating from a convective mechanism of rainfall generation, which is mainly caused by fronts associated with Mediterranean cyclones. In winter and spring, rainfall events are generally characterized by longer duration and lower intensity. Despite the necessity of assessing rainfall seasonality through mathematical approaches based on monthly precipitation (Feng et al., 2013; Nasta et al., 2020), the analysis of $\overline{R}_m$ reported in Fig. 3 can provide useful insights for evaluating the relative contribution of each season to the mean annual rainfall erosivity in a region. The results indicate that the mean summer (JAS) erosivity for the study area is approximately 25 % of $\overline{R}_a$ (25 %, 23 % and 28 % in Campania, Sardinia, and Sicily, respectively), while mean fall (OND) erosivity is about 45 % (42 %, 49 %, and

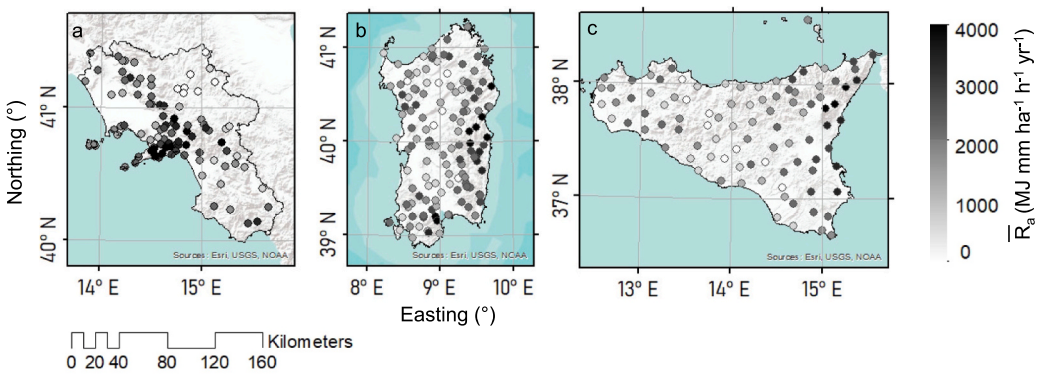


Fig. 2. Benchmark values of the mean annual rainfall erosivity, $\overline{R}_a$ (MJ mm ha^{-1} h^{-1} yr^{-1}), derived for each gauge station from high-resolution (10-min) rainfall data (Wischmeier and Smith, 1978) in a) Campania, b) Sardinia, c) Sicily.

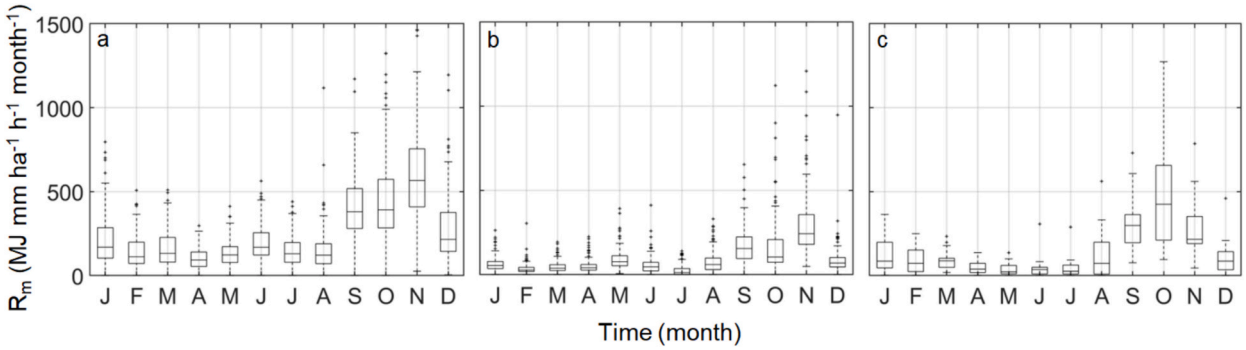


Fig. 3. Box-plots reporting the variability of the benchmark monthly rainfall erosivity values, $\overline{R}_m$ (MJ mm ha^{-1} h^{-1} month^{-1}) across all stations in a) Campania, b) Sardinia, and c) Sicily.

48 %, respectively). In contrast, approximately 16 % (18 %, 12 %, 17 % in Campania, Sardinia, and Sicily, respectively) of the mean annual erosivity $\overline{R}_a$ can be attributed to winter months (JFM) events, while the contribution of spring months (AMJ) events is approximately 14 % (15 %, 16 %, and 8 %, respectively). However, as illustrated in Fig. 3, the period from September to January, which is characterized by the occurrence of the most erosive storms, contributes, on average, to 67 % of the mean annual erosivity.

Following the split of the 335 rain gauges into calibration and validation datasets, a comparison was conducted based on the basic statistics of mean monthly rainfall and erosivity (Table 2). An analysis of variance (ANOVA) test (not reported for sake of brevity), at the 0.01 significance level, was then performed to verify the null hypothesis that the mean monthly precipitation, *MMP,* and the derived $\overline{R}_m$ remain the same for each month in the two datasets.

3.2. Mean annual rainfall erosivity from empirical equations

The ten existing empirical equations summarized in Table 1 were applied to the calibration ($n = 251$) and validation ($n = 84$) datasets. The comparison between the models was achieved by evaluating their performance against the validation dataset (Table 3).

As expected, the empirical equations using their original parametrization (without site-specific calibration) performed poorly (average RMSE of 1283 MJ mm ha^{-1} h^{-1} yr^{-1}). This is primarily attributed to the fact that they were developed for climatic conditions considerably different from our research area. Overall, the highest R^2_{adj} values were obtained by the two equations based on daily rainfall data (on average 0.83, vs. 0.70 and 0.63 achieved by monthly and annual-based formulations, respectively), which proved that daily rainfall erosivity models were in general more capable in explaining the variability of $\overline{R}_a$ across the various stations, compared to rainfall erosivity models based on coarser resolution. The ranking of the *KGE* values corroborated the excellent performance of F&P2014 and P&M2004. Only two equations (R&F1994 and OSZ2012) provided negative *KGE* values.

Therefore, formulations such as F&P2014 and P&M2004 are preferable when site-specific calibration is missing, leading to average absolute percentage errors in the estimation of $\overline{R}_a$ on the order of 34 %. In contrast, the monthly and annual rainfall erosivity models proved to be scarcely suitable for the study area, showing average absolute percentage error of 88 and 60 %, respectively.

Following the site-specific calibration process outlined in Section 2.5

Table 2
Mean monthly precipitation (*MMP*) and erosivity ($\overline{R}_m$) in mm and MJ mm ha^{-1} h^{-1} month^{-1}, respectively, over the calibration ($n = 251$) and validation ($n = 84$) datasets.

Data set	Month	J	F	M	A	M	J	J	A	S	O	N	D
CAL (n = 251)	*MMP*	90	75	79	50	44	23	9	11	55	74	130	89
	$\overline{R}_m$	134	85	103	70	93	104	72	112	304	348	392	151
VAL (n = 84)	*MMP*	92	75	81	51	43	22	10	11	57	76	124	88
	$\overline{R}_m$	118	80	91	73	86	99	83	98	308	356	370	130

Table 3
Number of predictors (x), number of parameters (p), parameter values (a, b, c, and d), for the empirical equations of Table 1. Models' performances (*RMSE*, R^2_{adj}, *ME*, *AIC*, *KGE*) achieved over the calibration (number of rain gauges $n = 251$) and validation ($n = 84$) datasets. Values within brackets refer to the original models, with the original parameters, while other values refer to recalibrated models. The best performances of the recalibrated models in each dataset for each indicator are highlighted in bold.

		Annual rainfall based equations					Monthly rainfall based equations					Daily rainfall based equations	
		FER2003	NAK2014	PAD2021	Y&R1996	R&F1994	ZHO1995	OSZ2012	FER1999	F&P2014	P&M2004	
	x	1	1	3	1	2	1	2	2	2	1	
	p	2	2	4	2	3	2	2	2	2	1	
	a	−732.64	*(−823.8)*	654.97	*(839.15)*	1.65	*(1.66)*	0.23	*(0.044)*	−11.16	*(95.77)*	3.25	*(−1.16)*	2.40	*(0.12)*	2.34	*(0.52)*	6.33	*(6.56)*	0.086	*(0.13)*
	b	3.26	*(5.21)*	0.0012	*(0.0008)*	−95.38	*(39.2)*	1.35	*(1.61)*	12.07	*(−6.081)*	−60.51	*(1.79)*	1.48	*(2.24)*	1.48	*(1.59)*	−73.69	*(−75.05)*		
	c					0.020	*(0.89)*			0.10	*(0.48)*										
	d					1.29	*(−0.63)*														
n = 251 (CAL)	*RMSE*	581	*(1833)*	595	*(851)*	505	*(1438)*	573	*(832)*	513	*(3196)*	586	*(923)*	514	*(2792)*	519	*(1557)*	**448**	*(436)*	545	*(1166)*
	R^2_{adj}	0.77	*(0.80)*	0.76	*(0.82)*	0.83	*(0.56)*	0.78	*(0.85)*	0.82	*(0.82)*	0.77	*(0.80)*	0.82	*(0.82)*	0.82	*(0.82)*	**0.87**	*(0.89)*	0.86	*(0.88)*
	AIC	2486	*(2934)*	2495	*(2635)*	2436	*(2844)*	2481	*(2626)*	2440	*(3153)*	2489	*(2667)*	2438	*(3094)*	2442	*(2871)*	**2382**	*(2374)*	2461	*(2756)*
	KGE	0.83	*(0.11)*	0.80	*(0.40)*	0.88	*(0.24)*	0.84	*(0.64)*	0.87	*(−1.04)*	0.83	*(0.42)*	0.87	*(−0.84)*	0.87	*(0.11)*	**0.93**	*(0.90)*	0.82	*(0.32)*
	ME	**0**	*(1617)*	15	*(−361)*	−2	*(−1166)*	−5	*(504)*	**0**	*(2230)*	**0**	*(−564)*	−3	*(1757)*	−3.43	*(−1318)*	−64	*(32)*	−179	*(768)*
n = 84 (VAL)	*RMSE*	593	*(1798)*	550	*(749)*	491	*(1354)*	566	*(797)*	509	*(2489)*	593	*(820)*	511	*(2077)*	509	*(1438)*	**412**	*(414)*	434	*(891)*
	R^2_{adj}	0.63	*(0.63)*	0.68	*(0.67)*	0.75	*(0.52)*	0.68	*(0.68)*	0.72	*(0.72)*	0.63	*(0.63)*	0.72	*(0.72)*	0.72	*(0.73)*	0.83	*(0.82)*	**0.84**	*(0.84)*
	AIC	1077	*(1263)*	1064	*(1116)*	1049	*(1219)*	1069	*(1126)*	1053	*(1320)*	1077	*(1131)*	1052	*(1287)*	1051	*(1226)*	**1016**	*(1016)*	1024	*(1143)*
	KGE	0.78	*(0.07)*	0.72	*(0.36)*	0.85	*(0.18)*	0.79	*(0.64)*	0.79	*(−0.77)*	0.78	*(0.40)*	0.80	*(−0.54)*	0.80	*(0.083)*	**0.90**	*(0.91)*	0.87	*(0.46)*
	ME	25	*(1581)*	**−21**	*(−299)*	93	*(−1159)*	48	*(398)*	−40	*(1835)*	25	*(−491)*	−29	*(1365)*	−33	*(−1252)*	−93	*(9)*	−189	*(625)*

(Table 3 and Fig. 4), all simplified equations improved significantly, achieving similar performance with each other. After recalibration, F&P2014 outperformed again all the other equations, with RMSE close to 400 MJ mm ha^{-1} h^{-1} yr^{-1}, R^2_{adj} higher than 0.80, KGE equal to 0.90, ME indicating a moderate bias with a slight underestimation of the R-factor, and the lowest AIC. The exponential model of P&M2004 ranked second and can be consistently enhanced by calibrating the exponent b at cost of a higher computational effort (Posch and Rekolainen, 1993; Yu and Rosewell, 1996b; Beguería et al., 2018). Overall, the two equations based on daily rainfall data obtained an average RMSE of 423 MJ mm ha^{-1} h^{-1} yr^{-1}, representing an average absolute percentage error of 22 %, and the best values of R^2_{adj}, KGE, and AIC.

The four equations based on monthly rainfall data obtained an average RMSE of 530 MJ mm ha^{-1} h^{-1} yr^{-1}, with an average absolute percentage error of 27 %. FER1999 was developed in one of the three pilot regions (i.e., Sicily) and obtained good performance with RMSE close to 500 MJ mm ha^{-1} h^{-1} yr^{-1}, R^2_{adj} higher than 0.70, KGE equal to 0.80, ME indicating a moderate bias, and the lowest AIC.

The four equations based on annual rainfall data obtained an average RMSE of 550 MJ mm ha^{-1} h^{-1} yr^{-1}, representing an average absolute percentage error of 28 %. PAD2021 was the best performing erosivity model in terms of all performance indicators among the annual rainfall models.

A visual inspection of the goodness-of-fit plots in Fig. 4 confirms the findings presented in Table 3, with data aligning well around the identity line, especially when $\overline{R}_a$ was estimated by using F&P2014. The other equations show higher dispersion, particularly for low $\overline{R}_a$ values. P&M2004 obtained the largest negative bias (ME = −189 MJ mm ha^{-1} h^{-1} yr^{-1}) as reported in previous studies (Angulo-Martínez and Beguería, 2009). We evidence the importance of recalibrating the empirical equations that in general halved the absolute percentage error from 60 to 26 %. R&F1994 obtained the larges reduction of the absolute percentage error from 128 to 26 %, with slight improvement of R^2_{adj} and KGE.

3.3. Performance of the new empirical equations ASAP1 and ASAP2

The first family of parsimonious models was subjected to a comprehensive examination of all nine possible combinations of the two predictors (REI and RII), as presented in Eqs. (4) and (5), to pinpoint the most suitable regression equation. Table 4 reports the resulting model performance indicators and displays the optimal parameter selection for each model. Again, the evaluation of the results presented below is exclusively based on the performance of the various models resulting with respect to the validation dataset. Overall, the nine models exhibited an average RMSE of 542 MJ mm ha^{-1} h^{-1} yr^{-1} (from 387 to 814 MJ mm ha^{-1} h^{-1} yr^{-1}) representing an average absolute percentage error of 28 %. However, models using RII (with one or two parameters) performed the worst. In contrast, REI-based models achieved a lower average RMSE of 497 MJ mm ha^{-1} h^{-1} yr^{-1}, slightly lower than the average RMSE obtained from the ten empirical models (Table 3). The best results, considering RMSE, R^2_{adj}, AIC, and KGE, were obtained with the three-parameter linear regression model (Eq. 14) using both REI and RII with intercept.

In light of these findings, we identified ASAP1 as the most suitable reference model under our parsimonious approach. This model, which was termed ASAP1 and demonstrated the best overall performance, exhibits the following analytical form with three parameters ($p = 3$):

$$\overline{R}_a = \beta_1 + \beta_2 \cdot REI + \beta_3 \cdot RII, \tag{14}$$

with $\beta_1 = -1317$, $\beta_2 = 7.7$ and $\beta_3 = 93.6$ after calibration (corresponding to the ensemble means over 1000 optimal parameter values, see Section 2.5).

In a second step we evaluated those regression equations that, beyond rainfall-based predictors, included easily derivable geographic

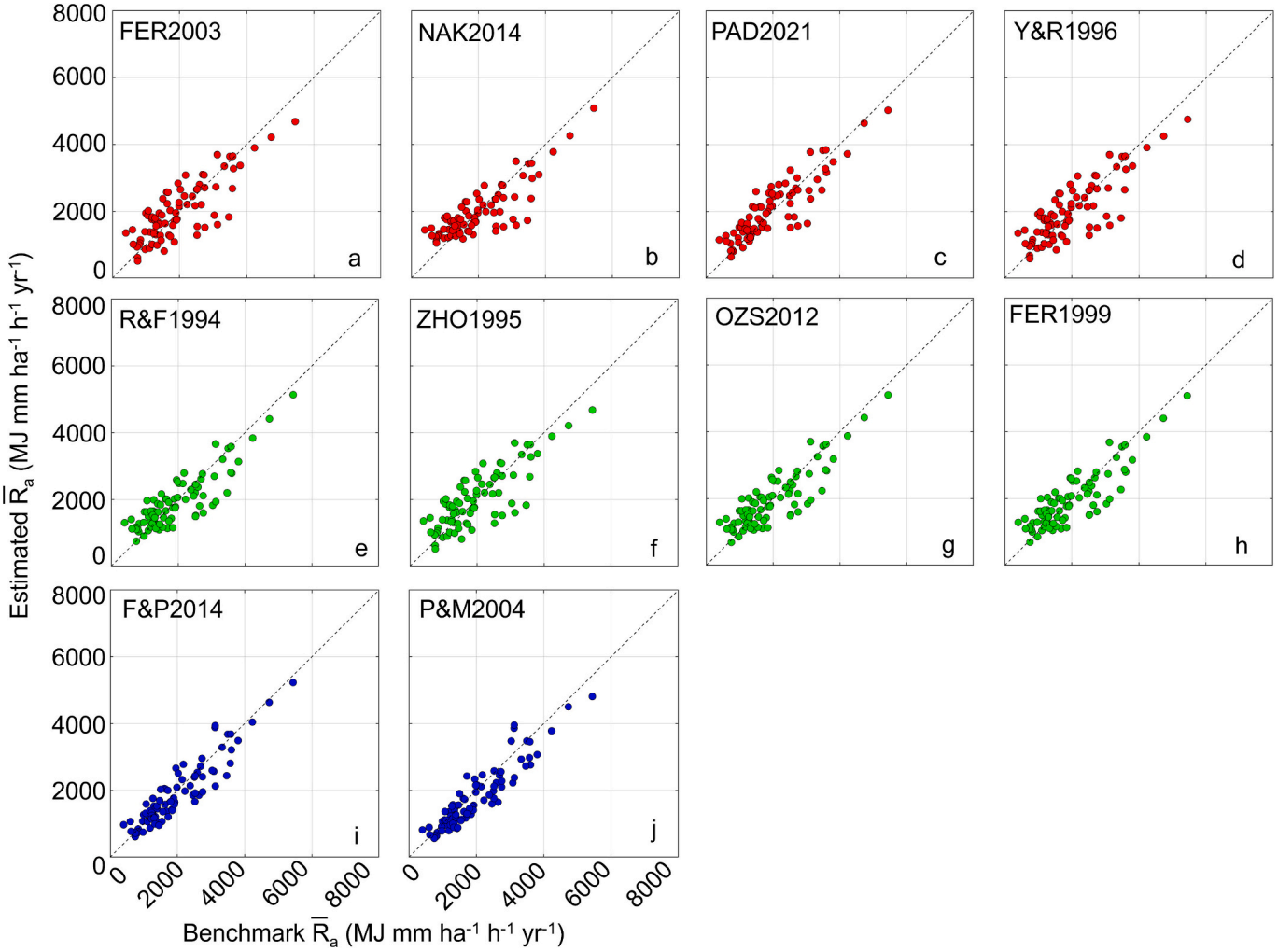


Fig. 4. Comparison between benchmark and estimated mean annual rainfall erosivity ($\overline{R}_a$) over the validation dataset ($n = 84$). Estimated $\overline{R}_a$ values were obtained with the ten empirical equations of Table 1, after recalibration in the study area. The equations are based on annual rainfall data (red circles): a) FER2003, b) NAK2014, c) PAD2021, d) Y&R1996, monthly rainfall data (green circles): e) R&F1994, f) ZHO1995, g) OZS2012, h) FER1999, daily rainfall data (blue circles): i) F&P2014, j) P&M2004. The 45° line depicts the perfect matching line (1:1 line).

Table 4
Number of predictors (x), number (p) of parameters β_1, β_2, and β_3, root mean square error (*RMSE*), adjusted coefficient of determination (R^2_{adj}), mean error (*ME*), Akaike Information Criterion (*AIC*), Kling-Gupta Efficiency (*KGE*), obtained by comparing the benchmark and simulated mean annual rainfall erosivity ($\overline{R}_a$) values in the calibration ($n = 251$) and validation ($n = 84$) datasets by different linear and nonlinear forms of ASAP1 based on the two compound rainfall-based variables (REI and RII). The best performances for each indicator are shown in bold for the validation dataset.

		$\beta_1 + \beta_2 \cdot$REI	$\beta_1 + \beta_2 \cdot$RII	$\beta_1 + \beta_2 \cdot$REI + $\beta_3 \cdot$RII	$\beta_1 \cdot$REI	$\beta_1 \cdot$RII	$\beta_1 \cdot$REI + $\beta_2 \cdot$RII	$\beta_1 \cdot$(REI)$^{\beta 2}$	$\beta_1 \cdot$(RII)$^{\beta 2}$	$\beta_1 \cdot$(REI)$^{\beta 2} \cdot$(RII)$^{\beta 3}$
	p	2	2	3	1	1	2	2	2	3
	β_1	402.74	−4612.99	−1939.72	11.22	94.51	8.70	31.24	1.01	2.21
	β_2	9.61	293.03	7.05			25.83	0.82	2.43	0.59
	β_3			122.35						1.23
n = 251 (CAL)	*RMSE*	475	685	372	527	973	442	477	750	373
	R^2_{adj}	0.85	0.68	0.91	0.85	0.68	0.87	0.85	0.62	0.90
	AIC	2408	2550	2314	2446	2685	2380	2409	2586	2315
	KGE	0.89	0.75	0.93	0.87	0.24	0.87	0.89	0.65	0.93
	ME	0	0	0	−128	103	29	−6	37	2
n = 84 (VAL)	*RMSE*	484	658	**387**	517	814	454	490	681	397
	R^2_{adj}	0.75	0.57	**0.84**	0.76	0.58	0.79	0.75	0.53	0.83
	AIC	1043	1094	**1007**	1052	1128	1032	1045	1100	1011
	KGE	0.84	0.74	**0.90**	0.85	0.24	0.82	0.85	0.62	0.88
	ME	**65**	111	74	−75	231	99	78	154	76

and terrain covariates as potential drivers for site-specific rainfall patterns.

The second equation, named ASAP2, was formulated using a trial-and-error method to determine the most effective analytical structure. This process entailed calibrating 242 simplified equations across the study area, each resulting from the combinations of five geographic and

terrain features, analyzed in both their linear and logarithmic forms. These equations were systematically constructed by incrementally adding terrain and geographic covariates to the two rainfall-based parameters (REI and RII) already present in ASAP1, as described by the following generic equation:

$$\overline{R}_a = \beta_1 + \beta_2 \cdot REI + \beta_3 \cdot RII + \beta_{p+3} \cdot x_{p+2}, \quad (15)$$

where x is the additional feature (*Lat*, *Z*, *AS*, *DS*, and *SL* or their logarithmic transformations) used as predictor, and p refers to the number of added covariates (ranging from 1 to 5). The parameters β_1, β_2 and β_3 were assumed to be equal to their optimal values derived for ASAP1. The 242 equations were ranked based on their AIC values, from highest (worst) to lowest (best). Fig. 5 illustrates the relationships between AIC and RMSE (Fig. 5a), and between R^2_{adj} and KGE (Fig. 5b), for the top-performing equations across the range of one to five terrain and geographical predictors. Table 5 provides a summary of these best equations, detailing their optimized parameters and resulting performance metrics.

The results indicate that the inclusion of up to three terrain and geographic features in Eq. (15) positively impacted model performance. Notably, the best model using a single terrain feature (*Z*) showed improved performance metrics, particularly a lower RMSE and a higher R^2_{adj}, compared to ASAP1. The most significant improvement was observed with the addition of three geographic and terrain features (*Z*, $\log_{10}DS$, and $\log_{10}Lat$), which enhanced all performance indicators. Models with two terrain features showed an RMSE between that of the best one-feature and three-feature models. Importantly, adding further geographic and terrain features beyond three (up to five) did not result in a substantial gain in predictive power over the three-feature combination. Therefore, we concluded that the equation utilizing the three terrain features offered the most effective compromise between model fit and parsimony. Thus, the erosivity equation based on three geographic and terrain features was assumed to be the best choice for ASAP2:

$$\overline{R}_a = \beta_1 + \beta_2 \cdot REI + \beta_3 \cdot \mathrm{RII} + \beta_4 \cdot Z + \beta_5 \cdot \log_{10} DS + \beta_6 \cdot \log_{10} Lat, \quad (16)$$

with $\beta_4 = -0.20$, $\beta_5 = -207.3$ and $\beta_6 = 187.2$ after calibration. Our analysis revealed that two of the three selected terrain features (*Z* and *Lat*) are consistent with those used in PAD2021, although ASAP2 incorporates the log-transformed version of latitude. This refined model, ASAP2, demonstrated a strong performance with an average absolute percentage error of 18 %.

Fig. 6 displays the goodness-of-fit plots comparing the benchmark and simulated R-factor values. In all cases, the scattered data align well around the identity line for the whole range of mean annual erosivity values that have been investigated. Despite its increased complexity, ASAP2 outperformed ASAP1 thanks to the inclusion of three terrain-based predictors. Importantly, all performance metrics in both the calibration and validation phases consistently confirmed that these three additional terrain predictors led to a marked improvement in the accuracy of the ASAP2 model.

Overall, our analysis supports that the easily-accessible geographic and terrain covariates (i.e., elevation, minimum distance to the sea, and latitude) improved information gain on storm variability, an important factor affecting rainfall erosivity.

In both ASAP1 and ASAP2, the regression hypotheses were examined and verified. For the sake of conciseness, results were not displayed. Plotting the residuals between benchmark and estimated mean annual erosivity values as a function of each predictor allowed for the verification of the first and second hypotheses. The Kolmogorov-Smirnov test proved that the residuals are normally distributed. Pearson correlation coefficients were used to assess cross-correlation among predictors, revealing that they were not highly correlated with one another. The highest observed correlation was between REI and RII ($r = 0.69$), which, while relatively strong, remains well below unity. Although this correlation is partially driven by the shared influence of MAP_{10}, it remains sufficiently low to suggest that multicollinearity is not a significant concern. This conclusion was further supported by the Variance Inflation Factor (VIF) value of 1.93, which is relatively close to the ideal value of 1.

4. Discussion

An accurate assessment of rainfall erosivity is crucial for understanding and mitigating soil erosion, a matter of significant environmental concern in vulnerable regions like the Mediterranean. However, obtaining reliable estimates of this key factor in the Mediterranean region is challenging primarily due to the limited availability and quality of fine high-resolution rainfall data from rain gauge networks (Fiener et al., 2013). This limitation hinders the precise calculation of rainfall erosivity. To overcome these limitations, researchers are increasingly exploring alternative data sources. One promising approach involves the use of satellite-based sub-hourly resolution rainfall products (Delgado et al., 2022). These products offer wider spatial coverage and finer temporal resolution than many rain gauge networks. However, a critical challenge associated with satellite data is the need for robust global validation to ensure their accuracy and reliability across different geographical and climatic conditions.

Another valuable alternative is the use of radar-derived rainfall

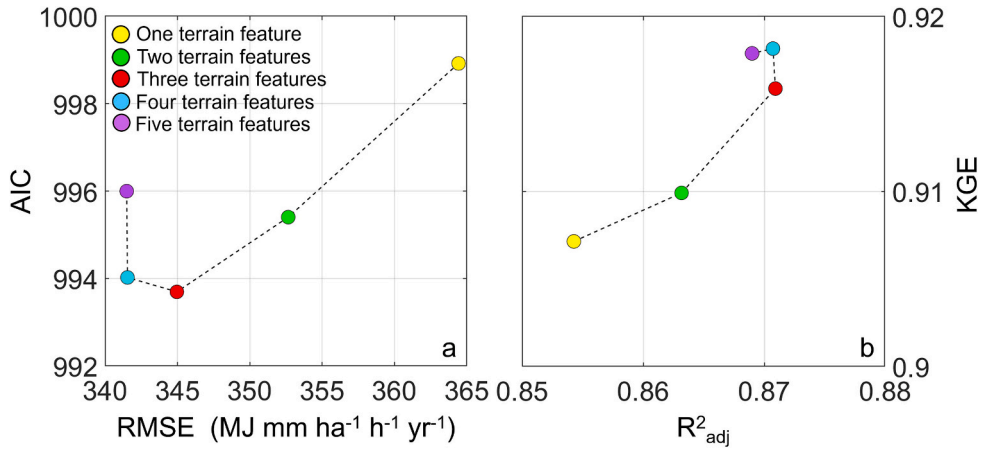


Fig. 5. Relationship between a) the root mean square error (*RMSE*) and the Akaike Information Criterion (*AIC*) and b) adjusted coefficient of determination (R^2_{adj}), and Kling-Gupta Efficiency (*KGE*) of the best combinations for fixed number of terrain features (from 1 to 5). Performance indicators refer to the validation data set ($n = 84$).

Table 5
Number of predictors (x), number (p) of parameters, root mean square error (*RMSE*), adjusted coefficient of determination (R^2_{adj}), mean error (*ME*), Akaike Information Criterion (*AIC*), Kling-Gupta Efficiency (*KGE*), of ASAP1 and the best analytical equations using one, two, three, four, and five geographic or topographic predictors for ASAP2. The performance indicators were obtained by comparing the benchmark and simulated mean annual rainfall erosivity ($\overline{R}_a$) values in the validation ($n = 84$) data set.

	x	p	Equation	*RMSE*	R^2_{adj}	*AIC*	*KGE*	*ME*
ASAP1	2	3	$-1317.02 + 7.66 \cdot REI + 93.60 \cdot RII$	387	0.84	1007	0.90	74
ASAP2	3	4	$-1317.02 + 7.66 \cdot REI + 93.60 \cdot RII - 0.15 \cdot Z$	364	0.85	999	0.91	16
	4	5	$-1317.02 + 7.66 \cdot REI + 93.60 \cdot RII - 0.34 \cdot Z + 112.99 \cdot \log_{10}(SL)$	353	0.86	995	0.91	40
	5	6	$-1317.02 + 7.66 \cdot REI + 93.60 \cdot RII - 0.20 \cdot Z - 207.32 \cdot \log_{10}(DS) + 187.17 \cdot \log_{10}(Lat)$	345	0.87	994	0.92	67
	6	7	$-1317.02 + 7.66 \cdot REI + 93.60 \cdot RII - 0.24 \cdot Z + 1.58 \cdot SL - 204.13 \cdot \log_{10}(DS) + 174.06 \cdot \log_{10}(Lat)$	342	0.87	994	0.92	59
	7	8	$-1317.02 + 7.66 \cdot REI + 93.60 \cdot RII - 0.24 \cdot Z + 1.46 \cdot SL + 40.97 \cdot AS - 205.36 \cdot \log_{10}(DS) + 164.98 \cdot \log_{10}(Lat)$	341	0.87	996	0.92	58

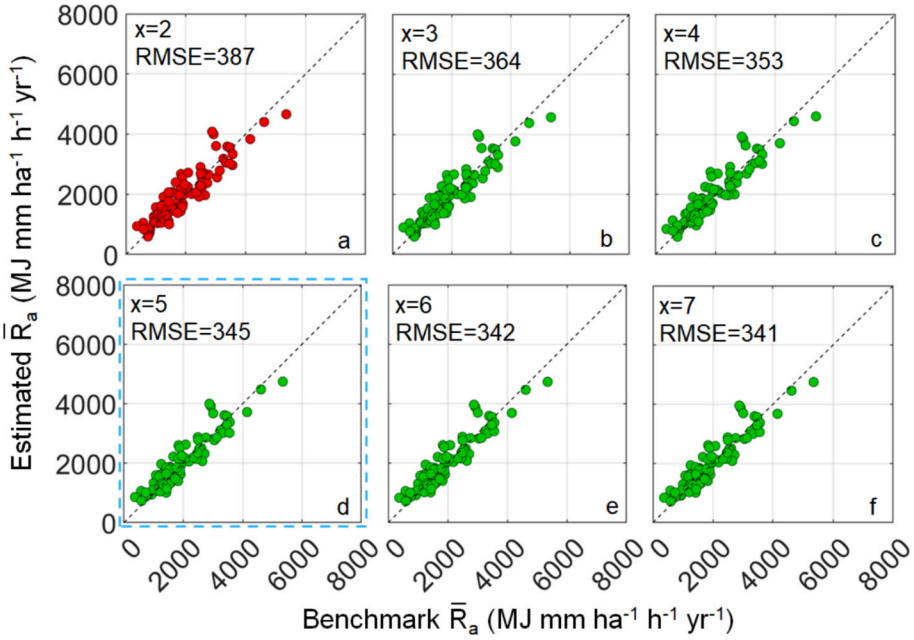


Fig. 6. Comparison between benchmark and estimated mean annual rainfall erosivity ($\overline{R}_a$) when using the validation data set ($n = 84$) relying on a) ASAP1 with two predictors (x = 2), b) ASAP2 with three predictors (x = 3), c) ASAP2 with four predictors (x = 4), b) ASAP2 with five predictors (x = 5), e) ASAP2 with six predictors (x = 6), f) ASAP2 with seven predictors (x = 7). The diagonal dashed line depicts the identity line (1:1 line). The root mean square error (RMSE) is reported in each subplot. The dashed cyan box identifies the best equation.

measurements, which are also gaining importance in estimating the R-factor (Auerswald et al., 2019). Rainfall radar systems can provide high-resolution spatial and temporal rainfall data over relatively large areas. Nevertheless, the widespread adoption of this technology is currently constrained by the limited spatial coverage of rainfall radar networks in many parts of the Mediterranean region.

Conversely, simplified empirical equations based on coarse resolution rainfall data offer a more readily available alternative for estimating rainfall erosivity. These equations often depend on readily accessible daily, monthly or annual rainfall data. The extensive datasets analyzed in this study enabled a more comprehensive validation process than previously achievable, potentially leading to significant improvements in the accuracy and reliability of erosivity assessments in the data-scarce contexts.

A central achievement of this study was the development of two new simplified equations for estimating rainfall erosivity. These equations demonstrated superior performance compared to ten existing equations after local recalibration. This suggests that ASAP1 incorporates key factors or relationships that previous approaches did not capture adequately. This improvement likely stems from a more refined representation of two rainfall characteristics that contribute most significantly to erosivity in the Mediterranean context: Rainfall Episodicity (REI) and Intensity (RII) Indices. The REI uses Gini's coefficient (G) to weigh MAP_{10} by describing the effect of precipitation intensity and distribution on the R-factor. Similarly, Bezak et al. (2021) analyzed the spatiotemporal distribution of more than 300,000 erosive events that were statistically described by resorting to Gini's coefficient. Bezak et al. (2021) found that higher G values corresponded to higher $\overline{R}_a$ values and interpreted that only few events contributed to the largest percentage of $\overline{R}_a$.

However, shortcomings could potentially occur in extreme situations. $G = 0$ represents a scenario in which rainfall is perfectly distributed throughout the year, whereas $G = 1$ corresponds to a case where the entire annual rainfall occurs on a single day. These two extreme cases are unrealistic in Mediterranean climates; therefore, the boundary values of G (0 and 1) should be understood as theoretical limits that G may approach under exceptional circumstances.

The Rainfall intensity index (RII) exploits two predictors, namely MAP_{10} and $\overline{d}_{10,a}$, by hypothesizing that higher rainfall erosivity values originate from more intense rainfall events concentrated within fewer rainfall days (Goovaerts, 1999). Yet, the use of RII alone in the parsimonious models proved to be inefficient in predicting the R-factor. The superior performances of the new models incorporating both REI and RII, compared to existing empirical equations, underscores the critical role of both the timing and magnitude of rainfall events in determining erosive potential. Although ASAP1 outperformed the ten empirical

equations in the study area, the negative value of the intercept in its equation might potentially lead to unrealistic negative values of mean annual rainfall erosivity in arid areas characterized by very low REI and RII values; therefore, it is highly recommended to recalibrate the regression parameters of ASAP1, especially in regions with low mean annual precipitation.

Furthermore, the study explored the relationship between rainfall erosivity and easily obtainable terrain and geographic features, such as elevation, minimum distance to the coastline, slope, aspect, and latitude. Specifically, in mountainous regions the elevation influences the amount of rainfall (Diodato and Bellocchi, 2007; Naipal et al., 2015; Nearing et al., 2015; Dallan et al., 2025). Similarly, the latitude and the shortest distance of rain gauge stations from the sea may have a relevant influence on the R-factor in coastal regions (Owen et al., 2011). The identification of correlations between these features and erosivity suggests that readily available spatial data can be used to further refine erosivity assessments, potentially even in areas with limited rainfall monitoring. This opens possibilities for developing spatially explicit models of erosivity that can be integrated into broader environmental assessments and land management planning. For instance, areas with steeper slopes or specific aspects might exhibit higher erosivity even with similar rainfall amounts, allowing for the prioritization of conservation efforts in these more vulnerable locations.

5. Concluding remarks

The generalizability of our findings hinges on two key factors: data representativity and the inherent complexity of empirical models. This study harnessed an extensive dataset to rigorously verify and validate both established and innovative empirical models for estimating rainfall erosivity, specifically addressing the data-scarce context of the Mediterranean region. Our analysis confirmed that increased model complexity generally correlates with enhanced performance, though this comes with the incorporation of additional parameters. Significantly, two newly developed empirical equations outperformed the ten most widely used existing simplified models, achieving this through local recalibration that reduced the average absolute percentage error from 27 % to 18 %. This advancement underscores the value of integrating novel rainfall-based features, such as rainfall episodicity and intensity indices, alongside readily available geographic and terrain features. Notably, models, both existing and new, that utilized daily rainfall data consistently yielded the best performance. Given these outcomes, we contend that a multi-model approach, or ensemble modeling, offers a more effective means of quantifying model generalizability than reliance on a single optimal model. This approach allows for the estimation of comprehensive uncertainty bands around predicted R-factor values, leading to a more reliable assessment of prediction accuracy. The robust performance of the proposed models within our three pilot regions, which exhibit considerable spatio-temporal variability in R-factor estimates and rainfall probability distributions, strongly indicates the potential for the models' transferability beyond the immediate spatial and temporal confines of our study, including under evolving climatic conditions.

The ensemble modeling approach would pave the way for analyzing temporal trends in both historical and projected rainfall erosivity, and for assessing the potential impacts of global warming. Climate change projections indicate an intensification of the Mediterranean region's hydrological cycle, which is anticipated to result in higher rainfall erosivity rates throughout the twenty-first century. The likely increase in the frequency and/or intensity of rainfall events will further exacerbate soil degradation, posing significant threats to agricultural productivity and water resources. Consequently, the development of accurate tools for assessing and predicting changes in rainfall erosivity is crucial for developing effective adaptation strategies.

Future research should prioritize the refinement of the proposed models, the integration of additional pertinent environmental factors, and the rigorous validation of their performance across a broader spectrum of Mediterranean environments to ensure their robustness and wider applicability. This ongoing effort will significantly enhance our capacity to accurately assess and effectively manage soil erosion, a critical challenge for the environmental sustainability of the Mediterranean region and beyond.

CRediT authorship contribution statement

Surafel M. Woldegebrael: Writing – original draft, Methodology, Data curation. **Nunzio Romano:** Supervision, Investigation, Conceptualization. **Dario Pumo:** Writing – review & editing, Writing – original draft, Methodology, Investigation, Data curation, Conceptualization. **Roberto Deidda:** Writing – review & editing, Writing – original draft, Methodology, Data curation, Conceptualization. **Matteo Ippolito:** Visualization, Software, Data curation. **Marcella Cannarozzo:** Writing – review & editing, Visualization, Formal analysis. **Andreas Langousis:** Writing – review & editing, Methodology, Conceptualization. **Athanasios V. Serafeim:** Formal analysis, Data curation, Conceptualization. **Salvatore Manfreda:** Writing – review & editing, Validation, Data curation. **Paolo Nasta:** Writing – review & editing, Writing – original draft, Validation, Supervision, Project administration, Methodology, Investigation, Funding acquisition, Data curation, Conceptualization.

Declaration of competing interest

The authors declare the following financial interests/personal relationships which may be considered as potential competing interests: Paolo Nasta reports financial support was provided by University of Napoli Federico II Department of Agricultural Sciences. Reports a relationship with that includes:. Has patent pending to. If there are other authors, they declare that they have no known competing financial interests or personal relationships that could have appeared to influence the work reported in this paper.

Acknowledgments

This study was carried out within the project ASAP ("Assessing and mapping novel agroecosystem vulnerability and resilience indicators in southern Italy", CUP E53D23021880001, Grant P20228L3KX) funded by European Union – Next Generation EU, Mission 4, Component C2, Investment 1.1 (PRIN 2022 PNRR, Call for tender No. 1409 published on 09.14.2022 by the Italian Ministry of University and Research). This study was also supported by financial resources from Next Generation EU and the Italian Ministry of University and Research through the PRIN PNRR 2022 project "An integrated modeling approach for mitigating climate change effects through enhanced weathering in Southern Italy" (CHANCES - CUP E53D23021850001, Grant P20225K9YW), and the RETURN Extended Partnership (CUP E63C22002000002, Grant PE0000005), under the European Union's Next Generation EU initiative (National Recovery and Resilience Plan - NRRP, Mission 4, Component 2, Investment 1.3 - D.D. 1243 of 02/08/2022). This manuscript reflects only the authors' views and opinions, and the Ministry cannot be considered responsible for them.

Data availability

Data will be made available on request.

References

Angulo-Martínez, M., Beguería, S., 2009. Estimating rainfall erosivity from daily precipitation records: a comparison among methods using data from the Ebro Basin (NE Spain). J. Hydrol. 379 (1–2), 111–121. https://doi.org/10.1016/j.jhydrol.2009.09.051.

Auerswald, K., Fischer, F.K., Winterrath, T., Brandhuber, R., 2019. Rain erosivity map for Germany derived from contiguous radar rain data. Hydrol. Earth Syst. Sci. 23, 1819–1832. https://doi.org/10.5194/hess-23-1819-2019.

Avino, A., Cimorelli, L., Furcolo, P., Noto, L.V., Pelosi, A., Pianese, D., Villani, P., Manfreda, S., 2024. Are rainfall extremes increasing in southern Italy? J. Hydrol. 631, 130684. https://doi.org/10.1016/j.jhydrol.2024.130684.

Ballabio, C., Borrelli, P., Spinoni, J., Meusburger, K., Michaelides, S., Beguería, S., et al., 2017. Mapping monthly rainfall erosivity in Europe. Sci. Total Environ. 579, 1298–1315. https://doi.org/10.1016/j.scitotenv.2016.11.123.

Beguería, S., Serrano-Notivoli, R., Tomas-Burguera, M., 2018. Computation of rainfall erosiv- ity from daily precipitation amounts. Sci. Total Environ. 637–638, 359–373. https://doi.org/10.1016/j.scitotenv.2018.04.400.

Benavidez, R., Jackson, B., Maxwell, D., Norton, K., 2018. A review of the (Revised) Universal Soil Loss Equation ((R)USLE): with a view to increasing its global applicability and improving soil loss estimates. Hydrol. Earth Syst. Sci. 22, 6059–6086. https://doi.org/10.5194/hess-22-6059-2018.

Bezak, N., Mikoš, M., Borrelli, P., Liakos, L., Panagos, P., 2021. An in-depth statistical analysis of the rainstorms erosivity in Europe. Catena 206, 105577. https://doi.org/10.1016/j.catena.2021.105577.

Bonilla, C.A., Vidal, K.L., 2011. Rainfall erosivity in Central Chile. J. Hydrol. 410 (1–2), 126–133. https://doi.org/10.1016/j.jhydrol.2011.09.022.

Dallan, E., Bagarello, V., Ferro, V., Pampalone, V., Borga, M., 2025. Evaluation and projected changes in rainfall erosivity: topography dependence revealed by convection-permitting climate projections for the Mediterranean island of Sicily. Catena 254, 108975. https://doi.org/10.1016/j.catena.2025.108975.

Delgado, D., Sadaoui, M., Ludwig, W., Méndez, W., 2022. Spatio-temporal assessment of rainfall erosivity in Ecuador based on RUSLE using satellite-based high frequency GPM-IMERG precipitation data. Catena 219, 106597. https://doi.org/10.1016/j.catena.2022.106597.

Deltas, G., 2003. The small-sample bias of the Gini coefficient: results and implications for empirical research. Rev. Econ. Stat. 85 (1), 226–234.

Diodato, N., Bellocchi, G., 2007. Estimating monthly (R)USLE climate input in a Mediterranean region using limited data. J. Hydrol. 345, 224–236.

Feng, X., Porporato, A., Rodriguez-Iturbe, I., 2013. Changes in rainfall seasonality in the tropics. Nat. Clim. Chang. 3 (9), 811–815.

Fernandez, C., Wu, J., McCool, D., Stoeckle, C., 2003. Estimating water erosion and sediment yield with GIS, RUSLE, and SEDD. J. Soil Water Conserv. 58, 128–136.

Ferreira, V., Panagopoulos, T., 2014. Seasonality of soil erosion under Mediterranean conditions at the Alqueva dam watershed. Environ. Manag. 54, 67–83. https://doi.org/10.1007/s00267-014-0281-3.

Ferro, V., Porto, P., Yu, B., 1999. A comparative study of rainfall erosivity estimation for southern Italy and southeastern Australia. Hydrol. Sci. J. 44 (1), 3–24.

Fiener, P., Neuhaus, P., Botschek, J., 2013. Long-term trends in rainfall erosivity – analysis of high resolution precipitation time series (1937–2007) from western Germany. Agric. For. Meteorol. 171-172, 115–123. https://doi.org/10.1016/j.agrformet.2012.11.011.

Gini, C., 1914. On the measurement of concentration and variability of characters. Metron 63, 3–38.

Goovaerts, P., 1999. Using elevation to aid the geostatistical mapping of rainfall erosivity. Catena 34, 227–242.

Johannsen, L.L., Schmaltz, E., Mitrovits, O., Klik, A., Smoliner, W., Wang, S., Strauss, P., 2022. An update of the spatial and temporal variability of rainfall erosivity (R-factor) for the Main agricultural production zones of Austria. Catena 215 (3), 1–14. https://doi.org/10.1016/j.catena.2022.106305.

Kottek, M., Grieser, J., Beck, C., Rudolf, B., Rubel, F., 2006. World map of the Köppen-Geiger climate classification updated. Meteorol. Z. 15, 259–263. https://doi.org/10.1127/0941-2948/2006/0130.

Loureiro, N.D.S., Coutinho, M.D.A., 2001. A new procedure to estimate the RUSLE EI_{30} index, based on monthly rainfall data and applied to the Algarve region, Portugal. J. Hydrol. 250, 12–18. https://doi.org/10.1016/S0022-1694(01)00387-0.

Montanarella, L., Panagos, P., 2021. The relevance of sustainable soil management within the European Green Deal. Land Use Policy 100, 104950. https://doi.org/10.1016/j.landusepol.2020.104950.

Naipal, V., Reick, C., Pongratz, J., Van Oost, K., 2015. Improving the global applicability of the RUSLE model – adjustment of the topographical and rainfall erosivity factors. Geosci. Model Dev. 8, 2893–2913. https://doi.org/10.5194/gmd-8-2893-2015.

Nakil, M., Khire, M., 2016. Effect of slope steepness parameter computations on soil loss estimation: review of methods using GIS. Geocarto Int. 31, 1078–1093. https://doi.org/10.1080/10106049.2015.1120349.

Nasta, P., Adane, Z., Lock, N., Houston, A., Gates, J.B., 2018. Links between episodic groundwater recharge rates and rainfall events classified according to stratiform-convective storm scoring: a plot-scale study in eastern Nebraska. Agric. For. Meteorol. 259, 154–161. https://doi.org/10.1016/j.agrformet.2018.05.003.

Nasta, P., Allocca, C., Deidda, R., Romano, N., 2020. Assessing the impact of seasonal-rainfall anomalies on catchment-scale water balance components. Hydrol. Earth Syst. Sci. 24, 1–17. https://doi.org/10.5194/hess-24-3211-2020.

Nearing, M.A., Unkrich, C.L., Goodrich, D.C., Nichols, M.H., Keefer, T.O., 2015. Temporal and elevation trends in rainfall erosivity on a 149 km^2 watershed in a semi-arid region of the American Southwest. Int. Soil Water Conserv. Res. 3 (2), 77–85.

Nearing, M.A., Yin, S., Borrelli, P., Polyakov, V.O., 2017. Rainfall erosivity: an historical review. Catena 157, 357–362. https://doi.org/10.1016/j.catena.2017.06.004.

Noto, L.V., Cipolla, G., Francipane, A., Pumo, D., 2023a. Climate change in the Mediterranean Basin (part I): induced alterations on climate forcings and hydrological processes. Water Resour. Manag. 37, 2287–2305. https://doi.org/10.1007/s11269-022-03400-0.

Noto, L.V., Cipolla, G., Pumo, D., Francipane, A., 2023b. Climate change in the Mediterranean Basin (part II): a review of challenges and uncertainties in climate change modeling and impact analyses. Water Resour. Manag. 37 (6–7), 2307–2323. https://doi.org/10.1007/s11269-023-03444-w.

Owen, J.J., Amundson, R., Dietrich, W.E., Nishiizumi, K., Sutter, B., Chong, G., 2011. The sensitivity of hillslope bedrock erosion to precipitation. Earth Surf. Process. Landf. 36 (1), 117–135.

Ozsoy, G., Aksoy, E., Dirim, M.S., Tumsavas, Z., 2012. Determination of soil erosion risk in the Mustafakemalpasa River Basin, Turkey, using the revised universal soil loss equation, geographic information system, and remote sensing. Environ. Manag. 50, 679–694.

Padulano, R., Rianna, G., Santini, M., 2021. Datasets and approaches for the estimation of rainfall erosivity over Italy: a comprehensive comparison study and a new method. J. Hydrol. Reg. Stud. 34, 100788. https://doi.org/10.1016/j.ejrh.2021.100788.

Panagos, P., Borrelli, P., Poesen, J., Ballabio, C., Lugato, E., Meusburger, K., Montanarella, L., Alewell, C., 2015a. The new assessment of soil loss by water erosion in Europe. Environ. Sci. Policy 54, 438–447.

Panagos, P., Ballabio, C., Borrelli, P., Meusburger, K., Klik, A., Rousseva, S., et al., 2015b. Rainfall erosivity in Europe. Sci. Total Environ. 511, 801–814.

Panagos, P., Vieira, D., Eekhout, J.P.C., Biddoccu, M., Cerdà, A., Evans, D.L., et al., 2024. How the EU Soil Observatory contributes to a stronger soil erosion community. Environ. Res. 248, 118319. https://doi.org/10.1016/j.envres.2024.118319.

Petkovšek, G., Mikoš, M., 2004. Estimating the R factor from daily rainfall data in the sub-Mediterranean climate of southwest Slovenia/Estimation du facteur R à partir de données journalières de pluie dans le climat sub-méditerranéen du Sud-Ouest de la Slovénie. Hydrol. Sci. J. 49 (5), 869–877. https://doi.org/10.1623/hysj.49.5.869.55134.

Piccarreta, M., Lazzari, M., Bentivenga, M., 2024. The influence in rainfall erosivity calculation by using different temporal resolution in Mediterranean area. Sci. Total Environ. 906, 167411. https://doi.org/10.1016/j.scitotenv.2023.167411.

Posch, M., Rekolainen, S., 1993. Erosivity factor in the universal soil loss equation estimated from Finnish rainfall data. Agric. Sci. Finl. 2, 271–279.

Prăvălie, R., Borrelli, P., Panagos, P., Ballabio, C., Lugato, E., Chappell, A., et al., 2024. A unifying modelling of multiple land degradation pathways in Europe. Nat. Commun. 15 (1), 3862. https://doi.org/10.1038/s41467-024-48252-x.

Renard, K.G., Freimund, J.R., 1994. Using monthly precipitation data to estimate the R-factor in the revised USLE. J. Hydrol. 157, 287–306.

Renard, K.G., Foster, G.R., Weesies, G.A., McCool, D.K., Yoder, D.C., 1997. Predicting Soil Erosion by Water: A Guide to Conservation Planning With the Revised Universal Soil Loss Equation (RUSLE). U.S. Department of Agriculture, Washington, DC, USA.

Richardson, C.W., Foster, G.R., Wright, D.A., 1983. Estimation of erosion index from daily rainfall amount. Trans. ASAE 26, 153–160.

USDA–ARS, 2013. Science Documentation: Revised Universal Soil Loss Equation Version 2. USDA–ARS, Washington, DC.

Wischmeier, W.H., Smith, D.D., 1978. Predicting rainfall erosion losses: a guide to conservation planning. In: Agric. Handb, 537. US Gov. Print. Office, Washington, DC.

Yin, S., Nearing, M.A., Borrelli, P., Xue, X., 2017. Rainfall erosivity: an overview of methodologies and applications. Vadose Zone J. 16 (12). https://doi.org/10.2136/vzj2017.06.0131.

Yu, B., Rosewell, C., 1996a. A robust estimator of the R-factor for the universal soil loss equation. Trans. ASAE 39 (2), 559–561.

Yu, B., Rosewell, C.J., 1996b. An assessment of daily rainfall erosivity model for New South Wales. Aust. J. Soil Res. 34, 139–152.

Zhou, F.J., Chen, M.H., Lin, F.X., Huang, Y.H., Lu, C.L., 1995. The rainfall erosivity index in Fujian Province. J. Soil Water Conserv. 9, 13–18.

Zhu, Z., Yu, B., 2015. Validation of rainfall erosivity estimators for mainland China. Trans. ASABE 58 (1), 61–71.